

# Trimodal Nanoparticle Contrast Agent for CT, MRI and SPECT Imaging: Synthesis and Characterization of Radiolabeled Core/Shell Iron Oxide@Gold Nanoparticles

Menachem Motiei,<sup>1,†</sup> Tamar Dreifuss,<sup>1,†</sup> Tamar Sadan,<sup>1</sup> Noam Omer,<sup>2</sup> Tamar Blumenfeld-Katzir,<sup>2</sup> Eirini Fragogeorgi,<sup>3</sup> George Loudos,<sup>3,4</sup> Rachela Popovtzer,<sup>\*1</sup> and Noam Ben-Eliezer<sup>2,5,6</sup>

<sup>1</sup>Faculty of Engineering and the Institutes of Nanotechnology and Advanced Materials, Bar-Ilan University, Ramat-Gan, Israel

<sup>2</sup>Department of Biomedical Engineering, Tel Aviv University, Tel Aviv, Israel

<sup>3</sup>Institute of Nuclear & Radiological Sciences, Technology, Energy & Safety, NCSR "Demokritos", Ag. Paraskevi 15310, Athens, Greece

<sup>4</sup>Bioemission Technology Solutions, Alexandras Avenue 116, 11472, Athens, Greece/Lefkippos Attica Technology Park NCSR "Demokritos", Ag. Paraskevi 15310, Athens, Greece

<sup>5</sup>Sagol School of Neuroscience, Tel Aviv University, Tel Aviv, Israel

<sup>6</sup>Center for Advanced Imaging Innovation and Research (CAI2R), New-York University Langone Medical Center, New York, NY, USA

E-mail: Rachela.Popovtzer@biu.ac.il

Recently, nanoparticles have emerged as promising contrast agents for various imaging applications. In this paper, we present the synthesis and characterization of a novel hybrid nano-structure, consisting of an iron oxide@gold nanoparticle, labeled with technetium-99m, for trimodal SPECT/CT/MRI imaging. The particles showed efficient capabilities as CT/MRI imaging agent and high radiochemical yield, indicating a potential single hybrid material for multimodal SPECT/CT/MRI.

**Keywords:** Multimodal imaging | Nanoparticle contrast agents | Core/shell nanoparticles

The idea of multimodal imaging, integrating two or more imaging modalities, has been emerging as a promising strategy for improving clinical and preclinical imaging.<sup>1–3</sup> Among the various clinically-used imaging techniques, computed tomography (CT), magnetic resonance imaging (MRI), and nuclear imaging are widely used for disease diagnosis, each providing different and complementary information about the patient. CT offers sensitivity to electron-dense elements such as bones, and delivers detailed anatomic information of the musculoskeletal system. However, it is limited in soft-tissue imaging applications. MRI enables detailed delineation of soft-tissue structures but it is less efficient in detecting lesions of bony structures.<sup>4</sup> Nuclear imaging, in particular single photon emission computed tomography (SPECT) and positron emission tomography (PET), offer the ability to track radiolabeled biomarkers with a very high detection sensitivity reaching below the picomolar range.<sup>5</sup> Yet, it suffers from poor spatial resolution, which led to the development of integrated SPECT or PET/CT and SPECT or PET/MRI scanners. The combination of these technologies allows each technique to recompense the limitations of the other, and provide complementary information with higher accuracy.

To further improve the sensitivity and specificity of the above imaging modalities, various types of contrast agents have been developed. Nanoparticles have emerged as a promising class of contrast agents for *in vivo* imaging applications, providing improved imaging and targeting capabilities compared to the commonly used contrast compounds.<sup>6–8</sup> Moreover, nanoparticles offer an efficient platform for multimodal imaging, by facilitating the combination of different imaging agents into one hybrid material.<sup>9</sup>

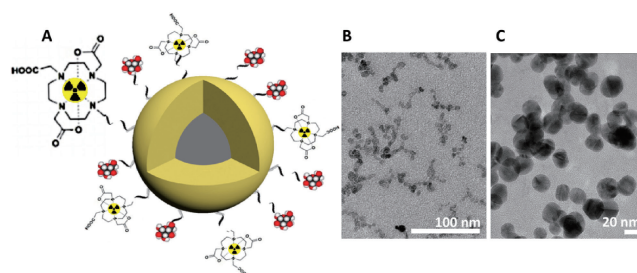


**Figure 1.** (A) Scheme of radiolabeled glucose-coated  $\text{Fe}_3\text{O}_4@Au$  nanoparticle. Iron oxide core (center, grey) is surrounded by a gold shell, coated with a polyethylene glycol linker (black curved lines), conjugated to glucose molecules (red-white), or to 1,4,7,10-tetraazacyclododecane-1,4,7,10-tetraacetic acid (DOTA) molecules (one molecule enlarged to illustrate its structure), as a chelating agent for the radioisotope (black-yellow, within DOTA). (B, C) Representative TEM images of (B)  $\gamma\text{-Fe}_3\text{O}_4$  core nanoparticles, with a mean diameter of  $8 \pm 2$  nm; scale bar = 100 nm (C) Final  $\text{Fe}_3\text{O}_4@Au$  nanoparticles; mean diameter 27 nm. Scale bar = 20 nm.

In the current study, we present a novel core/shell iron oxide@gold nanoparticle design (Figure 1A), with potential to be radiolabeled, and, as preliminary results indicate, suitable for CT, MRI, and SPECT imaging. While the magnetic iron oxide core serves to enhance MRI signal, the gold shell produces strong CT contrast. Although some Au and iron oxide hybrid nanoparticles were reported as CT/MRI contrast agents,<sup>10–14</sup> our new design offers higher Au mass ratio, precise control of the Fe/Au ratio, and ability to easily bind a variety of biological molecules to the particle surface. Moreover, our core/shell design further enables radiolabeling with various metal isotopes, thereby opening the door to trimodal CT-SPECT-MR imaging.

First, dextran T1-coated iron oxide nanoparticles were prepared according to a previously published method.<sup>15</sup> Briefly, a mixture of ferric chloride hexahydrate (3 g) and ferrous chloride tetrahydrate (1.5 g) in 32 mL deionized water was mixed with dextran T1 (Mw = 41 KDa) solution (1.7 g in 20 mL deionized water) for 30 min, at room temperature under nitrogen flow. The mixture was cooled to 5 °C, and ammonium hydroxide (28%, 12.7 g) was added under stirring over 2 min. Then, the mixture was heated to 60 °C for 40 min, and to 80 °C for 2 h. To allow

coating of the particles with a gold shell in the next steps, the dextran coating was removed and replaced by a citrate layer. This was done by washing the solid phase twice with 10% sodium citrate solution followed by centrifugation (4000 rpm, 20 min).

After purification, the iron oxide particles pellet was dissolved in 10% sodium citrate solution to yield a final Fe concentration of 4 mg/mL, as measured by flame atomic absorption spectroscopy (FAAS). The size and shape of the obtained iron oxide nanoparticles (IONPs) were determined using transmission electron microscopy (TEM), which indicated uniformly distributed, spherical nanoparticles, with a mean diameter of  $8 \pm 2$  nm (Figure 1B).

To form a gold shell on the IONPs, an Au solution (414  $\mu$ L of 50% w/V HAuCl<sub>4</sub> in 200 mL purified water) was heated until boiling, and 4.04 mL of the as-prepared IONP solution were added under stirring (10 min), yielding core-shell Fe<sub>3</sub>O<sub>4</sub>@Au nanoparticles. After cooling to room temperature, SH-PEG-COOH (1000 Da) solution (80  $\mu$ L, 36.5 mg/mL) was added followed by stirring for 3 h. The PEG molecules surround the particle surface via thiol–gold interactions, providing stability in physiological solutions and external active carboxylic group for further surface modifications. Next, the particles were coated by both glucose molecules and tetraazacyclododecane tetraacetic acid (DOTA) chelator. DOTA was used to enable radiolabeling, and the glucose coating was chosen as we have previously shown that it allows effective nanoparticle uptake by cells, *in vitro*, for cell tracking applications, and *in vivo*, for cancer diagnosis.<sup>16–21</sup> D-( $\beta$ )-glucosamine hydrochloride (30  $\mu$ L, 25 mg/mL) was added to the solution together with *N*-ethyl-*N*-(3-(dimethylamino)propyl) carbodiimide (EDC, 200  $\mu$ L, 10 mg/mL) and *N*-hydroxysuccinimide (NHS, 200  $\mu$ L, 10 mg/mL), followed by 3 h stirring at room temperature, to yield glucose-coated Fe<sub>3</sub>O<sub>4</sub>@Au nanoparticles. After purification, DOTA-NH<sub>2</sub> (1.3 mg) was added followed by 3 h stirring at room temperature. Finally, the solution was centrifuged to purify the nanoparticles. For the radioactive study, the particles were labeled with technetium-99m (<sup>99m</sup>Tc), due to its relatively long half-life, and its extensive use in clinics. Characterization was conducted using TEM, energy dispersive X-ray (EDAX), UV-Vis spectroscopy and dynamic light scattering (DLS), and radio TLC for the radiolabeled particles.

TEM image of the Fe<sub>3</sub>O<sub>4</sub>@Au nanoparticles (Figure 1C) demonstrated spherical nanoparticles, with a total mean diameter of 27 nm, indicating gold shell thickness of  $\sim$ 9.5 nm. The hydrodynamic diameter was  $\sim$ 140 nm, as measured by DLS. UV-vis spectra of Fe<sub>3</sub>O<sub>4</sub>@Au nanoparticles (Figure S1) demonstrated a surface plasmon resonance peak at 522 nm, corresponding to the typical peak of gold nanoparticles with similar size.

EDAX analysis, performed to analyze the composition of Fe<sub>3</sub>O<sub>4</sub>@Au nanoparticles and determine the Fe:Au ratio, confirmed the presence of both Fe and Au in the final nanoparticle, and indicated weight percentages of 3.8% and 96.2% for Fe and Au, respectively (Figure S2). This difference arises from the significantly larger mass of gold in the particle, together with the higher density of gold as compared to the iron oxide (19.32 g/mL vs. 5.24 g/mL, respectively). CT is limited by its low sensitivity to contrast agents, as compared with MRI and nuclear techniques.<sup>22</sup> X-ray attenuation of gold nanoparticles increases linearly with mass concentration, thus delivery of a greater mass concentration to sites of interest *in vivo* enables greater contrast enhancement.<sup>23</sup> The high gold-to-iron oxide mass ratio of our

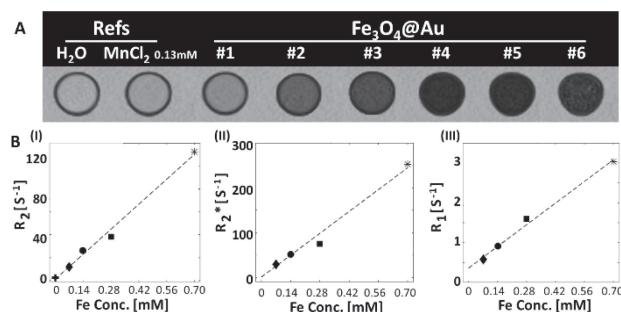


**Figure 2.** MRI dynamic contrast range of Fe<sub>3</sub>O<sub>4</sub>@Au nanoparticles. (A) MRI image of Fe<sub>3</sub>O<sub>4</sub>@Au nanoparticles at different Fe concentrations, #1–#6: 0.07, 0.14, 0.28, 0.70, 1.4, 2.1 mM. A positive contrast effect is seen with the increase of Fe<sub>3</sub>O<sub>4</sub>@Au nanoparticle concentration. (B) Quantification of Fe<sub>3</sub>O<sub>4</sub>@Au nanoparticle MR relaxation values in free-state. (I) R<sub>2</sub> (=1/T<sub>2</sub>) relaxation. (II) R<sub>2</sub>\* (=1/T<sub>2</sub>\*) relaxation, (III) R<sub>1</sub> (=1/T<sub>1</sub>) relaxation. Fe conc. shown up to 0.70 mM, as above this produced extremely rapid relaxation and very low signal at later echoes, preventing quantitative estimation of relaxation values.

nanoparticle is thus critically important for allowing efficient and simultaneous CT and MRI detection.

To evaluate the Fe<sub>3</sub>O<sub>4</sub>@Au nanoparticles as contrast agents for MRI, solutions at different Fe concentrations, ranging from 2.5  $\mu$ g/mL to 75  $\mu$ g/mL, were scanned on a 3 Tesla clinical MRI scanner (Siemens Prisma). Image contrast, evaluated using standard MRI protocols (see Supporting Information (SI)), showed an effective MR contrast for the assayed range of nanoparticle concentrations. Qualitative T<sub>2</sub>\* weighted MRI images (Figure 2A) show the nanoparticles' effectiveness in changing the image contrast compared to pure water and a manganese chloride (MnCl<sub>2</sub>) solution, which reduces the water relaxation values to a physiological range. Quantitative experiments were carried out to determine the accurate MR relaxation values of Fe<sub>3</sub>O<sub>4</sub>@Au nanoparticles in free-state.

All relaxation values decreased with an increasing nanoparticle concentration (Figure 2B), yielding the following range of values for the nanoparticle solutions: T<sub>2</sub> = 9...82 ms, T<sub>2</sub>\* = 4...34 ms, and T<sub>1</sub> = 330...1742 ms. These match the typical values used in human MRI scans, covering both healthy and pathological tissue values.<sup>24</sup>

Relaxivity values (in [mM<sup>-1</sup>sec<sup>-1</sup>]) were R<sub>1</sub> = 3.86, R<sub>2</sub> = 154.7, and R<sub>2</sub>\* = 346.6 (calculation in SI). Additionally, the concentration range of the MRI-active Fe compound is in accord with values reported in literature for *in vitro* models;<sup>25</sup> taken together with the relaxation values, this suggests that these Fe<sub>3</sub>O<sub>4</sub>@Au nanoparticles can generate contrast and enhance SNR in MR weighted imaging *in vivo*, even at low concentrations, which are more favorable for clinical use.

Next, the feasibility of Fe<sub>3</sub>O<sub>4</sub>@Au nanoparticles to be further used as CT contrast agents was assessed by scanning the same nanoparticle samples used for the MRI experiment in a micro-CT scanner (Skyscan High Resolution 1176; specifications in SI). Both Fe and Au concentrations of the samples were measured using FAAS (Figure 3). The slight difference between the weight percentages obtained by EDAX and FAAS is attributed to the different measurement technologies and their

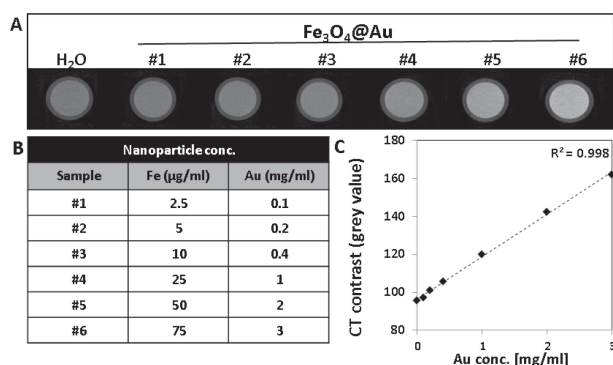


**Figure 3.**  $\text{Fe}_3\text{O}_4\text{@Au}$  nanoparticles as CT contrast agent. (A) CT images of  $\text{Fe}_3\text{O}_4\text{@Au}$  nanoparticles at different Au concentrations, ranging from 0.1 mg/mL to 3 mg/mL. (B) Summary of nanoparticle concentrations in the samples. (C) Correlation between CT signal intensity and gold concentration.

deviations. Figure 3 shows a clear visible contrast for nanoparticle samples with an Au concentration starting from 1 mg/mL. Quantification of the mean greyscale values demonstrated, as expected, a linear correlation between the observed CT contrast and the nanoparticle concentration. The lower sensitivity of the CT compared to the MRI to detect nanoparticles in small concentrations, highlights the importance of our large-thick-shell design, in which the Au volume is much higher than that of the  $\text{Fe}_3\text{O}_4$  core.

Preliminary experiments on radiolabeling of the DOTA-glucose-coated  $\text{Fe}_3\text{O}_4\text{@Au}$  nanoparticles were conducted, by radiolabeling with  $^{99\text{m}}\text{Tc}$  using the direct labelling approach,<sup>26,27</sup> in the presence of stannous chloride used as a reducing agent. This approach achieved a labelling incorporation as high as 98%.

The two-strip instant thin layer chromatography silica gel (ITLC-SG) method for analysis of  $^{99\text{m}}\text{Tc}$ -DOTA-glucose-coated  $\text{Fe}_3\text{O}_4\text{@Au}$  nanoparticles ( $^{99\text{m}}\text{Tc}$ -trimodal particle) showed that no amount of either pertechnetate ( $^{99\text{m}}\text{Tc}$ - $\text{TcO}_4^-$ ) (Figure 4A) or colloidal ( $^{99\text{m}}\text{Tc}$ - $\text{TcO}_2$ ) (Figure 4B) was present. Free pertechnetate was not determined when developed on acetone as eluent, as if there was any, it would migrate to the front of the ITLC-SG strip (retardation factor ( $R_f$ ) = 0.8–1.0), while leaving the reduced/hydrolyzed  $^{99\text{m}}\text{Tc}$ - $\text{TcO}_2$  ( $^{99\text{m}}\text{Tc}$ -colloids) and the  $^{99\text{m}}\text{Tc}$ -trimodal particle at the origin ( $R_f$  = 0.0).

Colloid formation was also undetected ( $R_f$  = 0.0) by using the same stationary phase (ITLC-SG), but a mobile phase of pyridine/acetic acid/water (3/5/1.5), where the  $^{99\text{m}}\text{Tc}$ -trimodal particle migrated to the front along with  $^{99\text{m}}\text{Tc}$ - $\text{TcO}_4^-$  ( $R_f$  = 1.0). With the combination of these two solvent systems, the percentage of the  $^{99\text{m}}\text{Tc}$ -trimodal particle derived and the radiochemical yield was higher than 98%, providing a single radioactive species. Stability tests showed stability up to 24 h post preparation.

DOTA-modified nanoparticles were radiolabeled by a straightforward methodology,<sup>26,27</sup> leading to a high complexation rate of  $^{99\text{m}}\text{Tc}$ . It is also notable that there was no need for further purification of the radiolabeled nanoparticles via a size exclusion column, a method previously used in a study based on a  $\text{Fe}_3\text{O}_4\text{-Au}$  particle<sup>28</sup> coated with various ligands and com-

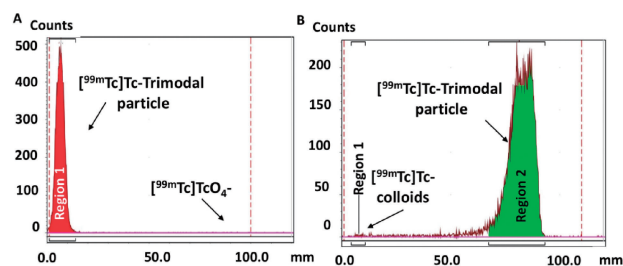


**Figure 4.** Radio TLC of  $^{99\text{m}}\text{Tc}$ -DOTA-glucose-coated  $\text{Fe}_3\text{O}_4\text{@Au}$  nanoparticles ( $^{99\text{m}}\text{Tc}$ -trimodal particle) developed on ITLC-SG chromatography paper with (A) acetone and (B) pyridine/acetic acid/water (3/5/1.5) as mobile phases.

plexed with  $^{99\text{m}}\text{Tc}(\text{I})$  via organometallic, tri-carbonyl chemistry, where the radiolabeling yield ranged between 24% to 52%<sup>28</sup> (which is lower than our result of >98%). Moreover, MRI and CT abilities of the above particle,<sup>28</sup> and of many other iron oxide core-gold shell nanoparticles (reviewed in ref 29) were not examined, possibly due to a relatively thin gold shell (ranging between 0.5–4 nm<sup>28,29</sup>) that likely would not enable CT imaging, due to the lower CT sensitivity to contrast agents,<sup>22</sup> necessitating a higher gold mass.<sup>23</sup> Composite dual-modal  $\text{Fe}_3\text{O}_4\text{-Au}$  particles<sup>30,31</sup> have been imaged, yet they lack the simpler spherical structure of our particles.

Others have shown multi-modal nanoparticles for CT, MRI and near-infrared imaging,<sup>32–34</sup> yet the latter modality has limited tissue penetration (<1–4 cm).<sup>35</sup> Using our approach, a single nanoparticle enables use of three different imaging modalities, all with deep tissue imaging abilities. Future studies will investigate the imaging efficacy *in vivo*. The variability in required concentrations between SPECT, CT and MRI can be easily circumvented by radioactively tagging only a fraction of the nanoparticles and creating mixtures with different relative amounts.

Altogether, the results demonstrate a highly effective nanoparticle, with a mean diameter of 27 nm, composed of a 8 nm-iron oxide core and a 9.5 nm-thick gold shell, with a proven efficacy as a dual-modal CT/MRI imaging agent and potential multi-modal SPECT/CT/MRI. The combination of these clinically-available imaging modalities in one system can enable scanning patients with all three systems on the same day, and following a single injection; it can also provide improved spatial, temporal and functional information. This particle is in the size range that we have previously shown to be optimal for *theranostics*—combined treatment and diagnostics.<sup>36,37</sup> We have previously designed gold nanoparticles conjugated to various moieties<sup>20,37,38</sup> for tumor targeting; moreover, the glucose coating enhances uptake by various cell types both *in vitro* and *in vivo*,<sup>16,20</sup> suggesting that the trimodal particles presented herein have potential to serve as a unique platform for precision imaging.

This project received funding from the European Union's Horizon 2020 research and innovation program under grant agreement #761031. This publication reflects only the author's views and the European Union is not liable for any use that may be made of the information contained herein. We thank the Ministry of Science and Technology, Israel for T.D.'s scholarship, and partial support by Stavros Niarchos Foundation



Industrial Scholarships, enhancing research in Greece. We thank Dr. Penelope Bouziotis, Research Director at the Radiochemical Studies Lab, for the radiolabeling studies at the National Center of Scientific Research “Demokritos”; and Chen Zror-Azankot for assistance with scheme creation.

Supporting Information is available on <https://doi.org/10.1246/cl.180780>.

## References and Notes

# M.M. and T.D. contributed equally to this work.

- 1 T. Dreifuss, E. Barnoy, M. Motiei, R. Popovtzer, *Theranostic Gold Nanoparticles for CT Imaging*, in *Design and Applications of Nanoparticles in Biomedical Imaging*, ed. by J. Bulte, M. Modo, Springer International Publishing, **2017**, pp. 403–427. doi:10.1007/978-3-319-42169-8\_19.
- 2 M. Poß, R. J. Tower, J. Napp, L. C. Appold, T. Lammers, F. Alves, C.-C. Glüer, S. Boretius, C. Feldmann, *Chem. Mater.* **2017**, *29*, 3547.
- 3 A. Gálisová, E. Fábryová, D. Jiráček, E. Sticová, A. Lodererová, V. Herynek, J. Kříž, M. Hájek, *Mol. Imaging Biol.* **2017**, *19*, 15.
- 4 W. Hou, F. Xia, G. Alfranca, H. Yan, X. Zhi, Y. Liu, C. Peng, C. Zhang, J. M. de la Fuente, D. Cui, *Biomaterials* **2017**, *120*, 103.
- 5 M. S. Judenhofer, H. F. Wehrl, D. F. Newport, C. Catana, S. B. Siegel, M. Becker, A. Thielscher, M. Kneilling, M. P. Lichy, M. Eichner, K. Klingel, G. Reischl, S. Widmaier, M. Röcken, R. E. Nutt, H.-J. Machulla, K. Uludag, S. R. Cherry, C. D. Claussen, B. J. Pichler, *Nat. Med.* **2008**, *14*, 459.
- 6 H. B. Na, I. C. Song, T. Hyeon, *Adv. Mater.* **2009**, *21*, 2133.
- 7 J. F. Hainfeld, D. N. Slatkin, T. M. Focella, H. M. Smilowitz, *Br. J. Radiol.* **2006**, *79*, 248.
- 8 M. A. Hahn, A. K. Singh, P. Sharma, S. C. Brown, B. M. Moudgil, *Anal. Bioanal. Chem.* **2011**, *399*, 3.
- 9 X. Li, X.-N. Zhang, X.-D. Li, J. Chang, *Cancer Biol. Med.* **2016**, *13*, 339.
- 10 H. Cai, K. Li, M. Shen, S. Wen, Y. Luo, C. Peng, G. Zhang, X. Shi, *J. Mater. Chem.* **2012**, *22*, 15110.
- 11 M. Yang, K. Cheng, S. Qi, H. Liu, Y. Jiang, H. Jiang, J. Li, K. Chen, H. Zhang, Z. Cheng, *Biomaterials* **2013**, *34*, 2796.
- 12 S. Narayanan, B. N. Sathy, U. Mony, M. Koyakutty, S. V. Nair, D. Menon, *ACS Appl. Mater. Interfaces* **2012**, *4*, 251.
- 13 J. Zhu, Y. Lu, Y. Li, J. Jiang, L. Cheng, Z. Liu, L. Guo, Y. Pan, H. Gu, *Nanoscale* **2014**, *6*, 199.
- 14 D. Kim, M. K. Yu, T. S. Lee, J. J. Park, Y. Y. Jeong, S. Jon, *Nanotechnology* **2011**, *22*, 155101.
- 15 K. G. Paul, T. B. Frigo, J. Y. Groman, E. V. Groman, *Bioconjugate Chem.* **2004**, *15*, 394.
- 16 O. Betzer, R. Meir, T. Dreifuss, K. Shamalov, M. Motiei, A. Schwartz, K. Baranes, C. J. Cohen, N. Shraga-Heled, R. Ofir, G. Yadid, R. Popovtzer, *Sci. Rep.* **2015**, *5*, 15400.
- 17 R. Meir, O. Betzer, M. Motiei, N. Kronfeld, C. Brodie, R. Popovtzer, *Nanomedicine: Nanotechnol., Biol. Med.* **2017**, *13*, 421.
- 18 O. Betzer, A. Schwartz, M. Motiei, G. Kazimirsky, I. Gispán, E. Damti, C. Brodie, G. Yadid, R. Popovtzer, *ACS Nano* **2014**, *8*, 9274.
- 19 R. Meir, K. Shamalov, O. Betzer, M. Motiei, M. Horovitz-Fried, R. Yehuda, A. Popovtzer, R. Popovtzer, C. J. Cohen, *ACS Nano* **2015**, *9*, 6363.
- 20 M. Motiei, T. Dreifuss, O. Betzer, H. Panet, A. Popovtzer, J. Santana, G. Abourbeh, E. Mishani, R. Popovtzer, *ACS Nano* **2016**, *10*, 3469.
- 21 T. Dreifuss, T.-S. Ben-Gal, K. Shamalov, A. Weiss, A. Jacob, T. Sadan, M. Motiei, R. Popovtzer, *Nanomedicine* **2018**, *13*, 1535.
- 22 D. P. Cormode, P. C. Naha, Z. A. Fayad, *Contrast Media Mol. Imaging* **2014**, *9*, 37.
- 23 L. E. Cole, R. D. Ross, J. M. Tilley, T. Vargo-Gogola, R. K. Roeder, *Nanomedicine* **2015**, *10*, 321.
- 24 G. J. Stanisz, E. E. Odobina, J. Pun, M. Escaravage, S. J. Graham, M. J. Bronskill, R. M. Henkelman, *Magn. Reson. Med.* **2005**, *54*, 507.
- 25 S. M. Vithanaratchi, M. J. Allen, *Curr. Mol. Imaging* **2012**, *1*, 12.
- 26 D. Psimadas, P. Bouziotis, P. Georgoulas, V. Valotassiou, T. Tsoitakos, G. Loudos, *Contrast Media Mol. Imaging* **2013**, *8*, 333.
- 27 A. Kostopoulou, K. Brintakis, E. Fragogeorgi, A. Anthousi, L. Manna, S. Begin-Colin, C. Billotey, A. Ranella, G. Loudos, I. Athanassakis, A. Lappas, *Nanomaterials* **2018**, *8*, 315.
- 28 M. Felber, R. Alberto, *Nanoscale* **2015**, *7*, 6653.
- 29 S. V. Salihov, Y. A. Ivanenkov, S. P. Krechetov, M. S. Veselov, N. V. Sviridenkova, A. G. Savchenko, N. L. Klyachko, Y. I. Golovin, N. V. Chufarova, E. K. Beloglazkina, A. G. Majouga, *J. Magn. Magn. Mater.* **2015**, *394*, 173.
- 30 J. Li, L. Zheng, H. Cai, W. Sun, M. Shen, G. Zhang, X. Shi, *ACS Appl. Mater. Interfaces* **2013**, *5*, 10357.
- 31 H. Cai, K. Li, J. Li, S. Wen, Q. Chen, M. Shen, L. Zheng, G. Zhang, X. Shi, *Small* **2015**, *11*, 4584.
- 32 M. M. van Schooneveld, D. P. Cormode, R. Koole, J. Timon van Wijngaarden, C. Calcagno, T. Skajaa, J. Hilhorst, D. C. 't Hart, Z. A. Fayad, W. J. M. Mulder, A. Meijerink, *Contrast Media Mol. Imaging* **2010**, *5*, 231.
- 33 J. Li, Y. Hu, J. Yang, P. Wei, W. Sun, M. Shen, G. Zhang, X. Shi, *Biomaterials* **2015**, *38*, 10.
- 34 J. C. Hsu, P. C. Naha, K. C. Lau, P. Chhour, R. Hastings, B. F. Moon, J. M. Stein, W. R. T. Witschey, E. S. McDonald, A. D. A. Maidment, D. P. Cormode, *Nanoscale* **2018**, *10*, 17236.
- 35 B. Zhu, E. M. Seveck-Muraca, *Br. J. Radiol.* **2015**, *88*, 20140547.
- 36 E. S. Davidi, T. Dreifuss, M. Motiei, E. Shai, D. Bragilovski, L. Lubimov, M. J. J. Kindler, A. Popovtzer, J. Don, R. Popovtzer, *Head Neck* **2018**, *40*, 70.
- 37 R. Meir, K. Shamalov, T. Sadan, M. Motiei, G. Yaari, C. J. Cohen, R. Popovtzer, *ACS Nano* **2017**, *11*, 11127.
- 38 I. Hazkani, M. Motiei, O. Betzer, T. Sadan, D. Bragilovski, L. Lubimov, A. Mizrahi, T. Hadar, M. Levi, I. Ben-Aharon, I. Haviv, R. Popovtzer, A. Popovtzer, *Theranostics* **2017**, *7*, 3962.